JOURNAL OF MATERIALS RESEARCH AND TECHNOLOGY 2021;12:2383–2395

Available online at www.sciencedirect.com

jmr&t Journal of Materials Research and Technology

journal homepage: www.elsevier.com/locate/jmrt

Original Article

Study of TiAl thin films on piezoelectric CTGS substrates as an alternative metallization system for high-temperature SAW devices

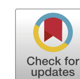

*Marietta Seifert**, *Eric Lattner, Siegfried B. Menzel, Steffen Oswald, Thomas Gemming*

Leibniz IFW Dresden, Helmholtzstr. 20, 01069, Dresden, Germany

ARTICLE INFO

Article history:
Received 25 November 2020
Accepted 5 April 2021
Available online 12 April 2021

Keywords:
TiAl multilayers
CTGS
Thin films
High-temperature SAW device

ABSTRACT

Ti/Al multilayer films with a total thickness of 200 nm were deposited on the high-temperature (HT) stable piezoelectric $Ca_3TaGa_3Si_2O_{14}$ (CTGS) as well as on thermally oxidized Si (SiO_2/Si) reference substrates. The Ti–Al films were characterized regarding their suitability as an alternative metallization for electrodes in HT surface acoustic wave devices. These films provide the advantage of significantly lower costs and in addition also a significantly lower density as compared to Pt, which allows a greater flexibility in device design. To realize a thermal stability of the films, AlNO cover as well as barrier layers at the interface to the substrate were applied. The samples were annealed for 10 h at up to 800 °C in high vacuum (HV) and at 600 °C in air and analyzed regarding the γ-TiAl phase formation, film morphology, and possible degradation. The Ti/Al films were prepared either by magnetron sputtering or by e-beam evaporation and the different behavior arising from the different deposition method was analyzed and discussed. For the evaporated Ti/Al films, AlNO barriers with a lower O content were used to evaluate the influence of the composition of the AlNO on the HT stability. The sputter-deposited Ti/Al films showed an improved γ-TiAl phase formation and HT stability (on SiO_2/Si up to 800 °C in HV and 600 °C in air, on CTGS with a slight oxidation after annealing at 800 °C in HV) as compared to the evaporated samples, which were only stable up to 600 °C in HV and in air.
© 2021 The Authors. Published by Elsevier B.V. This is an open access article under the CC BY license (http://creativecommons.org/licenses/by/4.0/).

1. Introduction

Engineering materials based on the intermetallic Ti–Al alloys are well established for high-temperature applications. They are used as bulk material or thick coatings, e.g., in aerospace structural components or in gas turbines [1,2]. In addition, because of their good high-temperature (HT) properties and oxidation resistance, Ti–Al alloy thin films became interesting as a material for electrodes in surface acoustic waves (SAW) devices, which are designed for operation at high temperatures. The search for metallizations which can be applied in

* Corresponding author.
E-mail address: marietta.seifert@ifw-dresden.de (M. Seifert).
https://doi.org/10.1016/j.jmrt.2021.04.006
2238-7854/© 2021 The Authors. Published by Elsevier B.V. This is an open access article under the CC BY license (http://creativecommons.org/licenses/by/4.0/).

such devices mainly has focused on materials based on noble metals as Pt and Pd [3–10], Rh/Ir [11], refractory metals [12,13], or RuAl [14–16]. Especially Pt, Ir, and also Ru are quite expensive materials and are therefore not the material of choice for an industrial application. In contrast to this, TiAl provides the advantage of significantly lower cost. In addition it also has lower density, which allows a greater flexibility in device design and can therefore open a field of further applications [17]. The advantage of lower mechanical losses and higher quality factors for low density Al as compared to Pt electrodes was described in detail by Streque et al. [18].

In former work we reported on 200 nm thick Ti–Al films deposited on thermally oxidized Si substrates, which were annealed up to 800 °C in high vacuum (HV) [17]. For some of the samples, a SiO_2 cover layer was used as an oxidation barrier against the ambient atmosphere. The results showed that the films with the SiO_2 cover layer were stable after annealing at 600 °C in HV. In contrast, films without the cover layer were strongly oxidized at this temperature. All films were destroyed after annealing at 800 °C. At this temperature, for all samples a strong chemical reaction between the Ti of the film and the SiO_2 of the substrate as well as the cover layer was observed, which resulted in the formation of a Ti silicide. Therefore, different cover and barrier layer materials have to be applied to realize both, the oxidation protection against the surrounding atmosphere, as well as a prevention of a chemical reaction between the film and the substrate. In this study, we investigated the suitability of AlNO as a protection layer.

The aim of this work was to develop Ti–Al based thin films for the application as a high-temperature electrode material in SAW sensors. As the substrate material, $Ca_3TaGa_3Si_2O_{14}$ (CTGS) was used since it is one of the most promising piezoelectric substrates for the use in HT SAW devices because it maintains its piezoelectric behavior almost up to its melting temperature of 1350 °C [19]. Thermally oxidized Si substrates (SiO_2/Si) served as a reference in this study.

2. Experimental

In our former work, Ti–Al alloy and Ti/Al multilayer (ML) thin films were prepared by sputter deposition on thermally oxidized Si substrates [17]. The annealing experiments showed that the desired γ-TiAl phase (tetragonal crystal structure, space group 123, $a \approx 2.83$ Å, $c \approx 4.08$ Å) was only formed in the multilayer samples. Therefore, this study focused on Ti/Al ML films (first layer Ti, top layer Al) with a total thickness of 200 nm. Details of the Ti/Al ML thin film preparation by sputter-deposition from elemental Al and Ti targets were described in [17]. For the sputter-deposited samples the individual layer thickness was 10 nm.

As already mentioned above, the final target of this investigation was to produce electrodes for SAW sensor devices, which means that the deposited Ti–Al films have to be structured to form the required interdigital transducer (IDT) array. A structuring procedure, which is widely applied in industry to realize SAW devices, is the low-cost lift-off technique. This means that prior to the film deposition, a photoresist mask (sacrificial layer) is prepared on the substrate, which represents the negative IDT pattern. Then the film is deposited and, subsequently, the sacrificial layer is removed, so that the positive structure of the IDTs remains on the substrate. A prerequisite for the successful removal of the photoresist is that the side edges of the photoresist mask are not covered by the deposited film. Since the technique of sputter-deposition results in a wide distribution of directions of the sputtered particles due to the relatively high gas pressure, a significant part of the material is also deposited on the side edges of the photoresist structures and complicates the lift-off process. In contrast to this, deposition by an evaporation technique is more oriented towards the forward direction. As a consequence, less material is grown on the side edges during the evaporation, which is beneficial for the lift-off process. Therefore, e-beam evaporation was evaluated as a second method of the preparation of the ML films. These depositions were done using two crucibles filled with Al and Ti ingots with a power of 495 and 141 W/mm^2 at a pressure of 1.2×10^{-6} and 3.8×10^{-7} mbar (substrate temperature = room temperature, RT). In case of the evaporation deposition, films with an individual layer thickness of 10 or 20 nm were compared.

CTGS (Fomos Materials, Russia) was used as the substrate material. However, it is known from experiments with RuAl thin films directly deposited on CTGS that chemical reactions between the substrate and the Al of the film take place during annealing at 800 °C in HV [20]. Therefore, Ti/Al films on thermally oxidized Si substrates (Active Business Company GmbH, Germany) were used as a reference, so that a comparison between both types of samples allows to determine the influence of the CTGS on the high-temperature behavior of the Ti/Al film.

Two kinds of AlN films with a different O content (denoted as AlNO) and a thickness of 20 nm were used as barrier layers between the substrate and the Ti/Al ML and on top of the layer stack. The AlNO films were prepared by RF sputtering from an AlN target. Using a mixture of Al and N_2 with the ratio of 40 sccm : 8 sccm as a sputtering gas resulted in an O content of about 16 at% (applied for the sputter-deposited Ti/Al ML samples), while a ratio of 44 sccm : 4 sccm led to a O content of about 8 at% (applied for the evaporated Ti/Al ML samples).

All depositions, the sputtering of the AlNO barriers and the sputtering as well as the evaporation of the Ti/Al MLs, were done in different chambers of the same cluster tool (CREAMET 350-CL 6, CREAVAC-Creative Vakuumbeschichtung GmbH, Dresden, Germany). A handling system allowed to transfer the samples between different chambers for the subsequent deposition steps without interruption of the HV. All metallic targets were supplied by J. Lesker Company with a purity of the metallic targets of at least 99.995 and AlN of 99.8.

To realize the γ-TiAl phase formation and to analyze the high-temperature behavior, the films were annealed at 600 or 800 °C in HV and at 600 °C in air for 10 h. In general, X-ray

diffraction (XRD) in Bragg–Brentano (BB) geometry is used to analyze the phase formation. However, in case of the samples prepared on CTGS the strong (0 3 0) diffraction peak of the single crystalline substrate at 2θ of 44.92° (Co-Kα radiation) overspreads the γ-TiAl (1 0 1) reflex at 45.27°, so that the γ-TiAl phase cannot be confirmed by BB-XRD on these substrates. An alternative procedure to determine crystallographic phases by X-ray diffraction is the measurement of pole figures. In contrast to the XRD in BB geometry, this method allows the measurement of tilted lattice planes, so that lattice planes without superposition with the CTGS can be selected and measured. The pole figure measurements were done with a Philips X'Pert MRD operating with Cu-Kα radiation (measurement steps of 2° in φ and ψ direction). To prove the formation of the γ-TiAl phase the two poles (1 0 1) at 2θ of 38.7° and (1 1 0) at 2θ of 45.3° were measured. For each pole figure measurement the actually used 2θ value was determined beforehand. This procedure was necessary since, due to variations in the composition or due to stresses in the film, the 2θ value of the respective sample can be slightly different from the theoretical one.

Depth profiles of the elemental distribution across the sample thickness were recorded using Auger electron spectroscopy (AES, JEOL JAMP-9500 Field Emission Auger Microprobe) in combination with Ar sputtering (energy of Ar ions: 1 keV with a current of 0.7×10^{-6} A). During this measurement the sample material was removed stepwise, and after each sputtering step the composition of the respective surface was determined from the measured AES spectra, resulting in a depth profile of the elemental concentration. An analysis of the peak shapes additionally allowed to draw conclusions on the oxidation state of the measured elements.

The method of quantification using standard single element sensitivity factors from the PHI-Multipak software [21] and the peak-to-peak height of the differentiated spectra was applied for the concentration determination. The results, however, allow only a coarse comparison of the samples, since the actual relative sensitivity factors of the elements in the alloys will be slightly different, and a preferential sputtering might lead to a demixing at the respective surface.

As an alternative method for the determination of the oxidation state of the elements present in the sample, X-ray photoelectron spectroscopy (XPS, PHI 5600 CI, Physical Electronics) was performed. Mg-Kα radiation (400 W) was used to excite the sample. A hemispherical detector with a pass energy of 29 eV was used to record the spectra. The depth profiles were realized by sputtering with Ar ions (3.5 keV). The C1s, O1s, N1s, Al2p, and Ti2p XP peaks were analyzed. Here also standard single element sensitivity factors from the PHI-Multipak software [21] were used, however, using the integrated peak areas of the spectra.

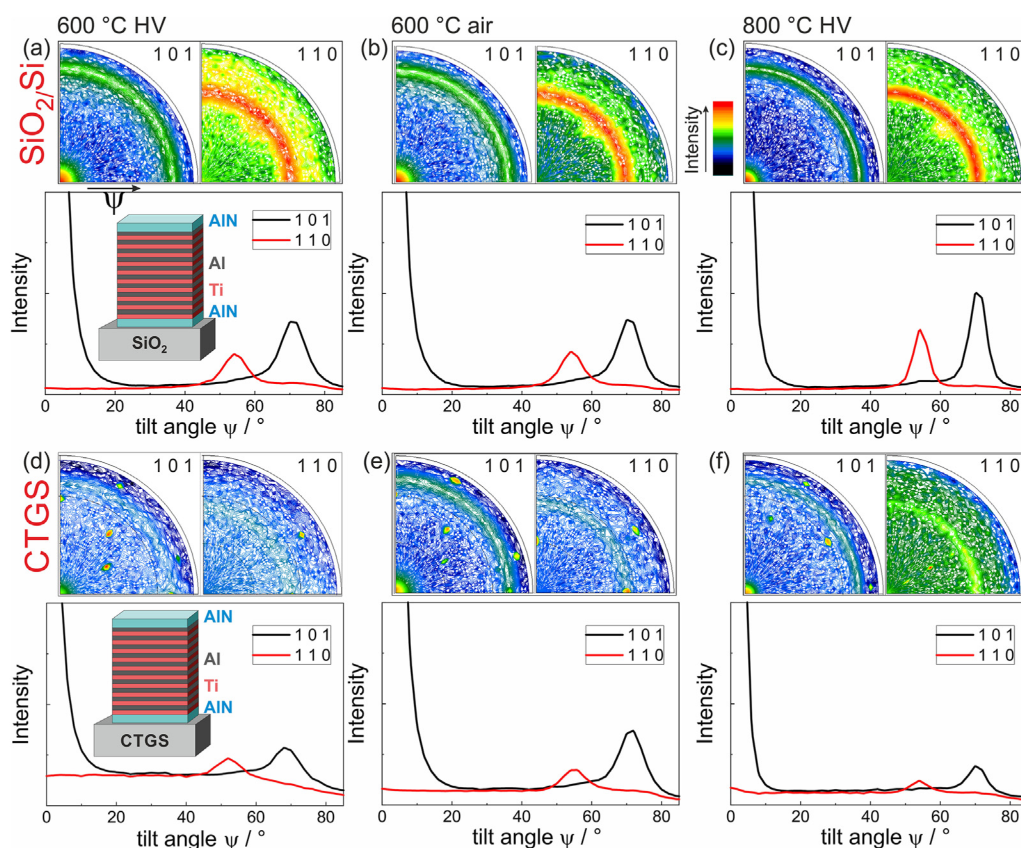

Fig. 1 – Results of the texture measurements of the sputtered Ti/Al ML samples on SiO_2/Si (upper row) and CTGS (lower row) after annealing for 10 h at (a,d) 600 °C in HV (b,e) 600 °C in air, and (c,f) 800 °C in HV (Texture plots were created using the software PANalytical X'Pert texture.)

Scanning electron microscopy (SEM) of the cross sections of the films prepared by the focussed ion beam technique (FIB, Zeiss 1540 XB Cross Beam, Carl Zeiss Microscopy GmbH, Oberkochen, Germany, SEM imaging in the same device) was performed to image the film morphology and, if present, the degradation after the heat treatment. Scanning transmission electron microscopy (STEM, Technai F30, FEI company, Hillsboro, OR, USA) was done to analyze the film morphology in more detail. Energy dispersive X-ray spectroscopy in the TEM (EDX, Octane T Optima, EDAX Company, Mahwah, NJ, USA) was used to determine the local composition of the samples. In addition, electron energy loss spectroscopy (EELS) was performed to analyze the chemical bonding.

3. Results

3.1. *Sputter-deposited Ti/Al multilayers*

3.1.1. *Phase formation*

Fig. 1 summarizes the results of the pole figure measurements of the sputtered samples on thermally oxidized Si and on CTGS substrates after the different annealing procedures. Independent on the annealing temperature or condition, the samples on SiO_2/Si showed a (1 0 1) γ-TiAl fibre texture with a strong intensity in the center of the pole figure and a corresponding circular ring at the tilt angle ψ of about 72°, which fits well (within the measurement step width) with the calculated angle of 71.18° between the {1 0 1} and {0 1 1} lattice planes. In agreement with this, the (1 1 0) pole figure contains a circular ring at ψ of about 54°, which corresponds well with the calculated angle of 54.41° between the {1 0 1} and {1 1 0} lattice planes. The formation of such a fibre texture was already observed in former work for Ti/Al ML on SiO_2/Si substrates covered with an SiO_2 layer after an annealing at 600 °C in HV [17].

Since the pole figures are scaled to their respective maximum, in addition the azimuthal averaged intensity versus the tilt angle ψ is plotted. A comparison of the three annealings for the films on SiO_2/Si showed that the highest intensity was measured for the sample annealed at 800 °C in HV (Fig. 1c). Both films annealed at 600 °C in HV (Fig. 1a) or air (Fig. 1b) had slightly lower but comparable intensities.

In contrast to the films on SiO_2/Si, the films on CTGS showed a reduced γ-TiAl phase formation. In the pole figures, in addition to the weak rings of the fibre texture, several strong individual peaks were visible. These originated from the CTGS substrate, which possesses several lattice planes with a lattice spacing comparable to the γ-TiAl (1 0 1) or (1 1 0) planes.

The difference in phase formation between samples deposited on SiO_2/Si and CTGS, despite the presence of the same amorphous barrier layer, was already observed for RuAl thin films [16].

3.1.2. *Film morphology*

In a first step, the film morphology and degradation were checked by SEM of cross sections prepared by the FIB technique. The images are summarized in Fig. 2. In the as-prepared state (Fig. 2a) the individual Ti and Al layers were hardly visible since their thickness was at the resolution limit of the imaging conditions. The AlNO layers appeared as bright lines below and above the Ti/Al layers due to charging effects. After annealing at 600 °C in HV or in air (Fig. 2b,c), for both substrates a homogeneous film was observed. However, for the air-annealed sample the film surface appeared slightly rougher. After annealing at 800 °C in HV, the film on SiO_2/Si was still intact, while in contrast to this the sample on the CTGS substrate was partly degraded (Fig. 2d). Bright grains were visible in the upper region of the film, which consisted most likely of Al_2O_3. In the surface region of the CTGS substrate degradation effects were also visible.

To determine interdiffusion and oxidation effects in the film during the annealing processes, AES depth profiles were measured. Fig. 3 summarizes the results for the ML samples on SiO_2/Si and CTGS in the as-prepared state and after the different annealing procedures.

Besides the already mentioned challenges with the unknown actual relative sensitivity factors for the quantitative evaluation of the AES measurements, there is another challenge for the evaluation of the AES spectra of the Ti–Al films with AlNO barrier. The elements Ti and N both possess AES peaks around an electron energy of 380 eV (N: 379 eV, Ti: 383 and 387 eV). Due to this overlap, the automated concentration evaluation wrongly results in a significant N content within the Ti/Al ML already in the as-deposited state. A detailed discussion on this topic was presented by Oswald et al. [22].

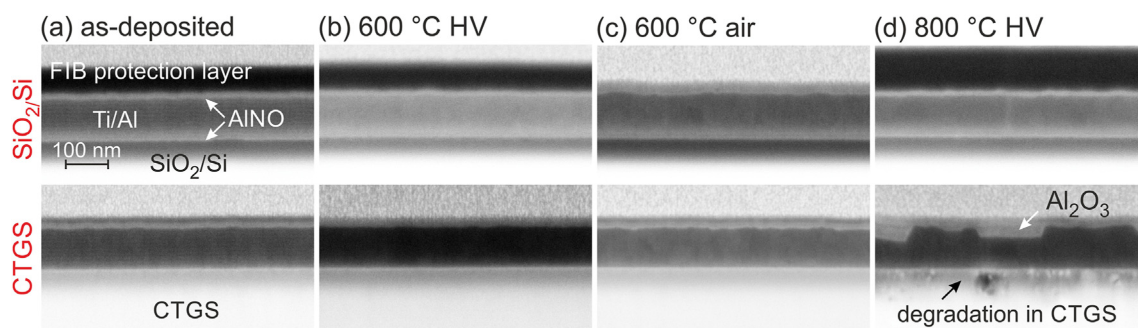

Fig. 2 – SEM images (3 kV, inLens) of the FIB cross sections of the sputtered Ti/Al ML samples on SiO_2/Si (upper row) and CTGS (lower row) (a) in the as-prepared state and after annealing for 10 h at (b) 600 °C in HV, (c) 600 °C in air, and (d) 800 °C in HV.

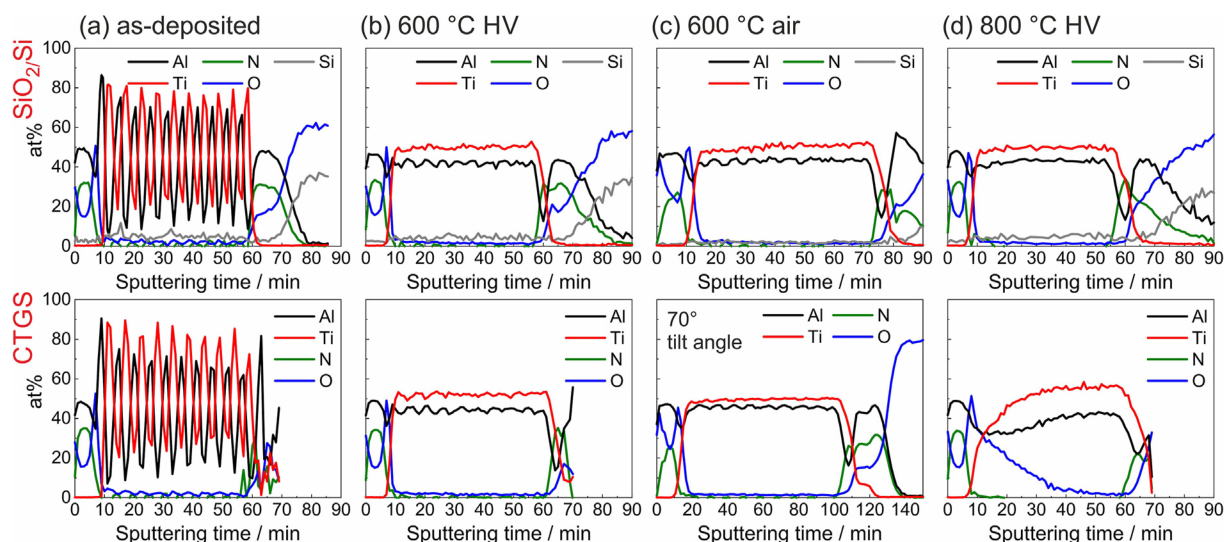

Fig. 3 – AES depth profiles (Ar ion energy: 1 keV) of the sputtered Ti/Al ML samples on SiO_2/Si (upper row) and CTGS (lower row) (a) in the as-prepared state and after annealing for 10 h at (b) 600 °C in HV, (c) 600 °C in air, and (d) 800 °C in HV. The measurement of the CTGS sample annealed at 600 °C in air was performed with a tilt angle of 70°, which resulted in a lower charging and allowed the measurement also of the bottom AlNO layer.

The fraction of the real N KLL signal was determined by analyzing the ratio of the Ti LMV (418 eV) and Ti LMM peak (387/383 eV, overlapping with the N KLL position) in a pure N-free Ti region of the film. This procedure led to a reasonable N atomic concentration in the AlNO barrier layers. On the other hand, due to the fitting of noisy peaks the calculated N signal, within the accuracy limit, takes a small negative value at certain positions. Another point, which complicates the AES evaluation, is the strong charging of the insulating CTGS substrate during the measurement.

In Fig. 3a the results of the AES measurement of the sputtered films on SiO_2/Si and CTGS in the as-prepared state are shown. In the AlNO cover layer a strong O signal of about 30 at % at the film surface and 15 at% in the center of the layer was measured. The O signal increased again approaching the uppermost Al layer of the Ti/Al ML. For AlNO films it is known that their morphology depends on the O content as, e.g., described by Brien and Pigeat [23]. According to the phase diagram they determined, AlNO layers with an O content of above 15 at% are expected to be amorphous. Amorphous cover layers are especially suited as oxidation barriers due to the lack of fast diffusion paths along grain boundaries.

Below the AlNO cover layer the sequence of the individual Al and Ti layers was clearly resolved by the AES measurement. A difference between the films on the two substrates became obvious when the interface to the substrate was reached during the stepwise sputtering. In case of the films on SiO_2/Si it was possible to measure the bottom AlNO layer as well as the substrate itself. In contrast to this, in case of the CTGS substrate the bottommost Al layer was still measured, but afterwards only noise was detected. This was due to the strong charging of the insulating CTGS substrate, which made it more or less impossible to analyze the bottom AlNO layer and the substrate itself by the used yield optimized AES setup [22].

Fig. 3b presents the results of the AES measurements of the samples after annealing at 600 °C in HV. The samples on both substrates showed a similar behavior. There was a complete interdiffusion of the Ti and Al, resulting in a homogeneously mixed Ti–Al layer. There was no change of the AlNO layer at the surface of the sample. At the interface to the bottom AlNO layer it can be seen that the Al signal decreased prior to the Ti signal and that simultaneously the N signal increased prior to the O signal. The presence of N within the bottom-most Ti layer indicated a reaction between the Ti and the AlNO.

The chemical reaction between Ti and AlN layers or bulk material was subject of many publications due to the importance of AlN as a coating material or in packaging applications in combination with Ti or Ti-based alloys [24,25]. It was described that the free energy of formation of TiN is more negative than that of AlN, leading to a decomposition of the AlN and the formation of $TiAl_3$ and of Ti–N phases at the interface. The experiments dealt with bulk material or thick films, above 100 nm, and to our knowledge there is no literature on the reaction of very thin AlN and Ti layers. Nevertheless, the described mechanisms of the reaction of Ti with AlN will also take place in very thin layers, which explains the strong N signal measured in the bottom Ti layer.

The AES results of the sputtered samples annealed at 600 °C in air are shown in Fig. 3c. For the samples on both substrates it could be seen that there was again a homogeneous Ti–Al layer without any oxidation. In both cases, a N signal was observed in the Ti–Al layer at the interface to

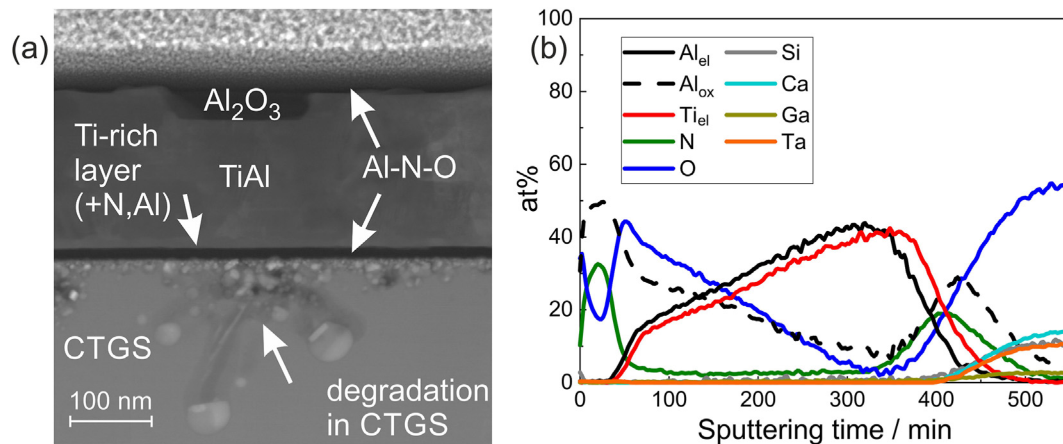

Fig. 4 – Ti/Al ML sample (prepared by sputtering) on CTGS after annealing at 800 °C in HV for 10 h: (a) STEM image with predominant elemental contrast and (b) XPS depth profile (el = elemental, ox = oxidized, the oxidation state was determined for Ti and Al).

the lower AlNO. In contrast to the samples annealed in HV, the composition of the covering AlNO layer had changed. There was an increase in the O and a decrease in the N content. An EDX analysis of a TEM lamella resulted in a composition of about $Al_{30}N_{20}O_{50}$. Locally, some small Al oxide grains with a size of a few nm were found below the cover layer. An AES measurement with a tilt angle of 70° was done for the sample on CTGS annealed at 600 °C in air. At this tilt the charging was reduced and it became possible to measure the AlNO bottom layer at the cost of an unstable sputter rate. The analysis of the interface between the Ti/Al and the bottom AlNO layer showed that its composition corresponded almost to that of the film in the as-prepared state.

The measurements of the samples annealed at 800 °C in HV demonstrated the influence of the CTGS substrate (Fig. 3d). While there was a homogeneous Ti–Al layer in the sample deposited on SiO_2/Si, the sample on CTGS possessed a significant O content in the upper region of the film. The AlNO cover layer appeared unchanged.

It is known from former work on RuAl thin films that during annealing at 800 °C in HV a strong reaction takes place between the CTGS and a RuAl film directly deposited on it. O and Ga diffuse out of the substrate, leading to an oxidation of the Al in the lower region of the film [20]. We also revealed that an AlNO barrier layer is not suited as an oxidation protection for RuAl thin films during annealing at 900 °C in HV, nevertheless it successfully acts as diffusion barrier between the CTGS and the RuAl and as a cover layer during annealing at 600 °C in air [16]. However, as mentioned above, the combination of AlNO with Ti leads to additional reactions.

A degradation of the upper region of the CTGS substrate was visible in the cross section image of the sample annealed at 800 °C in HV shown in Fig. 2d. This finding indicated that there was a reaction between the film on top and the substrate.

For this sample, a STEM and EDX analysis was performed. In the STEM image in Fig. 4a the distribution of the damages in the CTGS substrate is demonstrated. There was a continuous degraded zone with a thickness of a few ten nm, and locally there were degradations up to a depth of several 100 nm. EDX analyses showed that the dark grain in the upper region of the Ti–Al film consisted of Al_2O_3, and that the thin layer (few nm) on top of the bottom AlNO layer was Ti-rich and containing some N and only a very small amount of O. To reveal whether Ti and Al were present in the elemental or oxidized state, XPS measurements were performed. An XPS depth profile of this sample is presented in Fig. 4b. Ti was only present in an elemental state (denoted as Ti_{el}). Oxidized Al (Al_{ox}) was found in both barrier layers. The signal of oxidized Al measured below the top AlNO layer corresponded to the Al_2O_3 grains, which were seen in the STEM image. In the lower region of the film, unoxidized Al and Ti were present. Again, it can be seen that the Al_{el} signal decreases prior to the Ti signal and that the N signal increases prior to the O signal of the bottom AlNO layer. With XPS, however, it is not possible to prove the formation of TiN, since the shift of the Ti peak in the TiN phase as compared to elemental Ti is too low to be resolved by this technique.

EDX measurements revealed that there was still a continuous AlNO layer on top of the substrate with a composition of about $Al_{40}N_{30}O_{30}$. Above this layer there was a Ti-rich $Ti_{60}Al_{40}$ layer. We assumed that the O, which was released due to the decomposition of the CTGS substrate, diffused through the Ti–Al layer until it reached the covering AlNO layer where it led to the formation of Al oxide below it. This oxide formation cannot arise from O diffusing through the cover layer since the protection against the environment was the same for the samples on both substrates, and such an effect was not observed for the sample on SiO_2/Si.

The analysis of the interface between the Ti–Al layer and the bottom AlNO layer revealed that a higher amount of N is diffused into the bottom Ti layer as compared to the samples annealed at 600 °C. The higher annealing temperature led to a stronger reaction between the Ti and the AlNO.

A determination whether N was solved in the Ti-rich layer or if a Ti–N phase was formed was possible by analyzing the EELS N–K-edge. Fig. 5 shows the EELS N–K-edge measured at two positions in the sample annealed at 800 °C in HV: in the Ti-rich layer on top of the bottom AlNO layer and in the AlNO

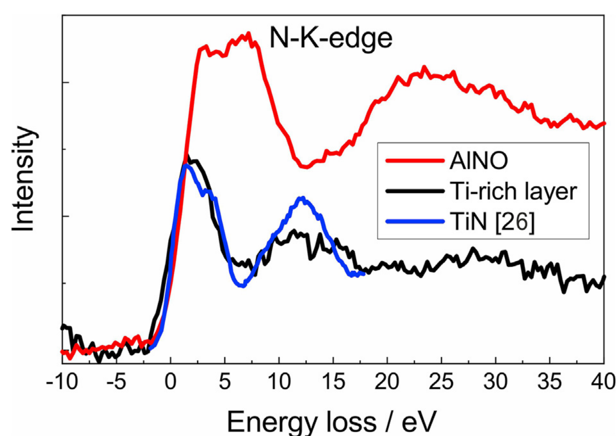

Fig. 5 – Results of the EELS measurements (sputtered sample annealed at 800 °C in HV) of the EELS N–K-edge measured in the Ti-rich layer at the interface to the bottom AlNO (black) and in the AlNO layer (red). In blue, the N–K-edge measured by Lazar et al. for a TiN layer is added for comparison [26].

layer itself. For comparison, the signal measured by Lazar et al. for a TiN layer is shown [26]. The results clearly revealed that the signal measured in the Ti-rich layer was similar to that reported in literature for the TiN phase, which confirms that also in our thin layers a reaction between Ti and AlN took place, leading to the formation of Ti–N phases. The shape of the N–K-edge of the AlNO layer differs strongly and fits well with the data measured by Pankov et al. for an AlN film [27].

3.2. *Evaporated Ti/Al multilayers*

In the second part of this work evaporated Ti/Al ML samples were analyzed. For these samples, in addition, a slightly different AlNO layer with a reduced O content was used to determine the influence of the O content on the high-temperature stability of the Ti–Al film. The comparison of the γ-TiAl phase formation for the evaporated and sputter-deposited samples was done with the films annealed at 600 °C in HV.

3.2.1. *Phase formation*

The results of the pole figure measurements of the evaporated Ti/Al ML samples on SiO_2/Si or CTGS after annealing at 600 °C in HV or in air are summarized in Fig. 6. In the upper row, the results for the films with 10 nm and in the lower row with 20 nm individual layer thickness are shown. It could be seen that for all films with 10 nm individual layer thickness, independent on the substrate or annealing condition, the γ-TiAl phase was formed with a low intensity (Fig. 6a–d). As for the sputtered films, the phase formation of the films annealed in air was comparable to that of those annealed in HV. In the pole figure images of the samples on CTGS (Fig. 6b and d) the (1 0 1) fibre texture appeared considerably weaker; however, this was due to the scaling of the images to the maximum value and the high intensity peaks of the CTGS reflexes, which were simultaneously detected.

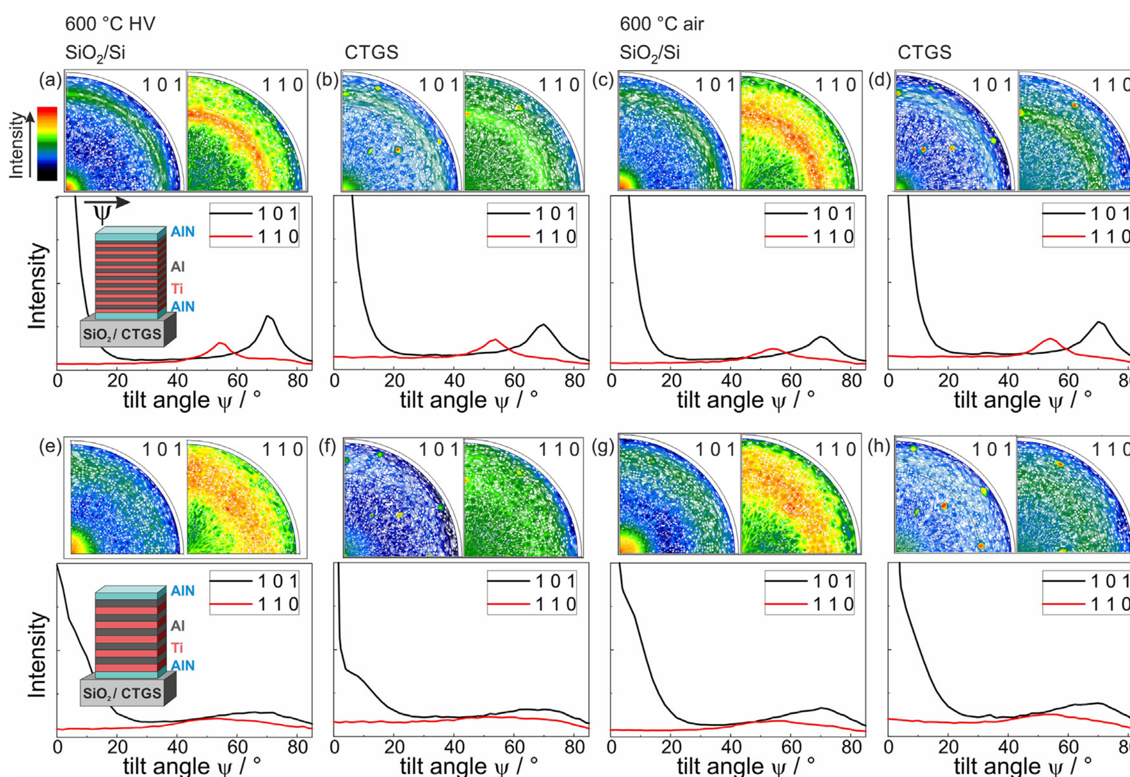

Fig. 6 – Results of the texture measurements of the evaporated Ti/Al ML samples on SiO_2/Si or CTGS after annealing at 600 °C in HV or in air for 10 h (a–d) ML with 10 nm and (e–h) with 20 nm individual layer thickness (Texture plots were created using the software PANalytical X'Pert texture.)

A comparison with the results shown in Fig. 1 for the sputtered Ti/Al ML films after annealing at 600 °C revealed that the phase formation of the sputtered samples was stronger for the films on SiO_2/Si. The fibre texture showed a higher intensity with a smaller full width at half maximum. For the films on CTGS, the difference in phase formation between both deposition techniques was reduced.

The films with 20 nm layer thickness showed hardly any phase formation (Fig. 6e-h). In contrast to this, in former work on sputtered Ti/Al ML with 10 and 20 nm individual layer thickness on SiO_2/Si substrates with SiO_2 cover layers, we found a comparable phase formation for both kinds of samples [17]. Obviously, this was different for the evaporated films.

In contrast to the results for the sputter deposited ML shown in Fig. 1, for the evaporated films no phase formation at all was detected for the samples annealed at 800 °C in HV.

3.2.2. *Film morphology*

For the evaporated films AES depth profiles were measured as well. Fig. 7 presents the results for the samples after annealing at 600 °C in HV and in air. In contrast to the sputter deposited films, it was not possible to measure AES depth profiles for the evaporated films after annealing at 800 °C in HV. Obviously, the charging during the measurement was too strong to allow a sputter removal of the film, which indicated a severe oxidation of the samples.

The measurements of the samples annealed at 600 °C in HV proof the lower O content of the AlNO barrier layers, which is about 8 at%. The small variations of the Al and Ti signal, especially visible in Fig. 7 a, b, e, and f, originated from the accuracy of the measurement and were also influenced by the required mathematical separation of the superimposed Ti and N intensity, which was described in Section 3.1.2.

All films annealed at 600 °C, independent on the layer stack, substrate, or annealing condition, almost had the same layer structure. At the lower interface between the bottom Ti and AlNO layer, as for the sputter deposited films, a Ti rich layer containing N was found. The reaction between Ti and AlNO leading to the formation of Ti–N also took place for the AlNO with the lower O content. It was visible that this Ti–N rich bottom layer was slightly thicker for the films with 20 nm individual layer thickness (Fig. 7e,f). Concurrently, the Ti content in the Ti–Al layer was slightly lower. This was explained by the larger amount of Ti, which was bound to N and therefore lacked within the Ti–Al film.

All films annealed in air (Fig. 7c,d,g,h) had a higher O content in the AlNO cover layer. For the sputter deposited samples, a higher O signal was measured as well; however, there was a clear maximum at the surface and at the interface to the Ti–Al layer. The latter was not seen for the evaporated samples. There was an almost continuous decrease in the O signal instead. In addition, the evaporated films annealed at 600 °C in air showed an O signal in the upper region of the Ti–Al layer in contrast to the films annealed in HV. This effect was not seen in the sputter deposited samples.

SEM images of the FIB cross sections of the evaporated samples with 10 or 20 nm individual layer thickness after the various heat treatments are summarized in Fig. 8. After annealing at 600 °C in HV (Fig. 8a), all films appeared homogeneous and no severe degradation was visible. In contrast to the sputter deposited films, locally small pores were observed.

The SEM images of the FIB cross sections of the samples annealed at 600 °C in air revealed that the films were still intact to a large extend (Fig. 8b). Besides some small pores, Al_2O_3 grains were present mainly in the upper part of the film, which was in agreement with the O signal in the AES measurements within the first minutes of sputtering of the Ti–Al layer of these films (Fig. 7c,d,g,h).

After annealing at 800 °C in HV (Fig. 8c), all samples were strongly degraded. The strong oxidation, which was proven by TEM and EDX analyses, explained the lack of TiAl XRD reflexes

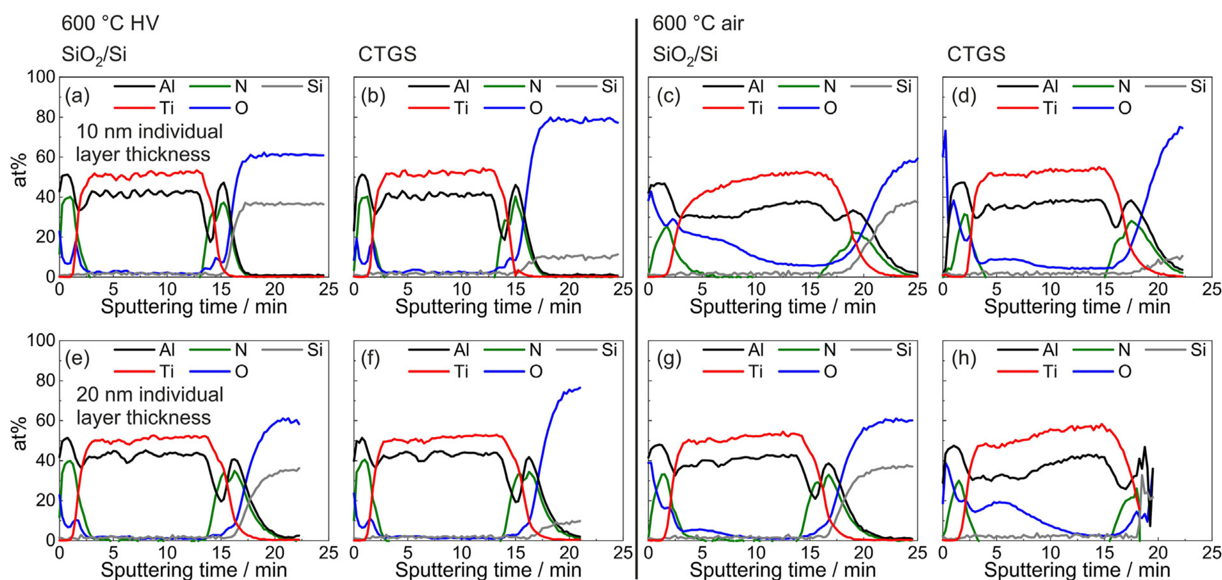

Fig. 7 – Results of the AES depth profiles for the evaporated Ti/Al ML on SiO_2/Si or CTGS after annealing at 600 °C in HV or in air for 10 h (a–d) ML with 10 nm and (e–h) with 20 nm individual layer thickness.

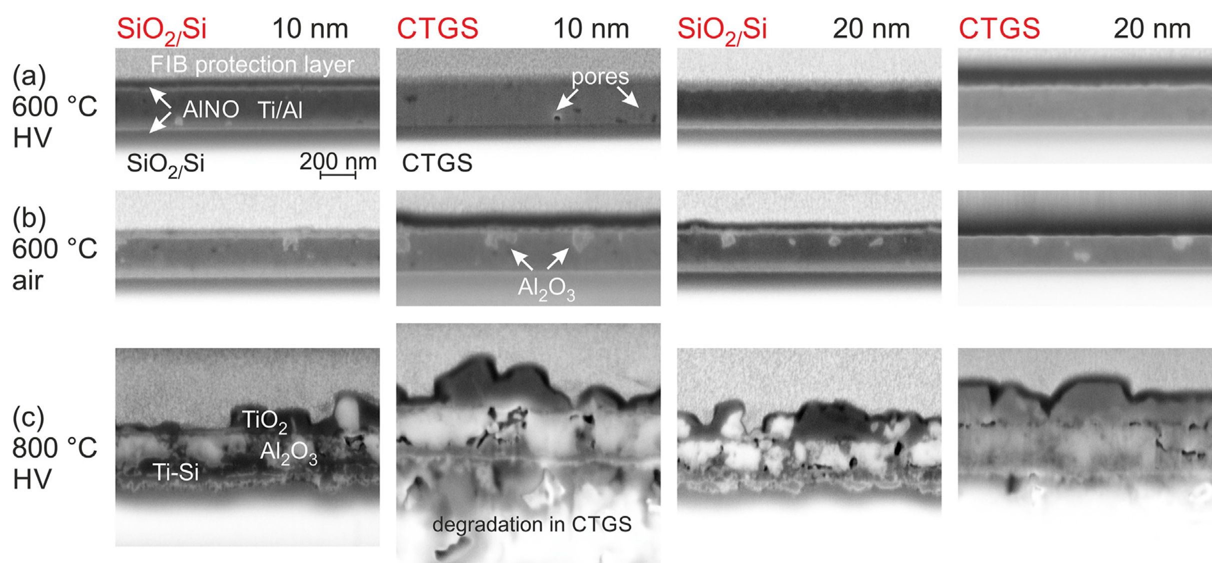

Fig. 8 – SEM images (3 kV, inLens) of the FIB cross sections of the evaporated Ti/Al ML samples on SiO_2/Si and CTGS with 10 or 20 nm individual layer thickness after annealing for 10 h at (a) 600 °C in HV, (b) 600 °C in air, and (c) 800 °C in HV.

and the difficulties in measuring AES depth profiles. The upper region of the SiO_2/Si substrate at the interface to the film was slightly degraded, while there was a severe degradation in the upper region of the CTGS substrate up to a depth of about 1 μm. The films also contained a lot of pores. In the images of Fig. 8c, the upper and lower boundary of the former Ti–Al layer were still recognizable. It appeared that on top of this layer separate grains had formed.

To analyze the local composition of the film after the heat treatment, an EDX mapping was done in the TEM for the Ti/Al ML sample with 10 nm individual layer thickness on SiO_2/Si after annealing at 800 °C in HV. The results of the EDX intensity mapping are shown in Fig. 9. The analyses revealed that the grains on top of the film consisted of Ti–O. In the region of the former Ti–Al layer mainly Al_2O_3 was present. On top of the interface to the substrate, at some locations, a Si signal was present in the region where Ti was also measured. Simultaneously, the O signal was reduced there. Also below the former interface to the substrate, strong Ti and Si signals were measured in the same region. This indicated the formation of a Ti silicide. The reaction between Ti and SiO_2 was already observed in former work on Ti/Al ML directly deposited on thermally oxidized Si substrates [17]. During the annealing of these samples at 600 or 800 °C, at the interface between the substrate and the Ti–Al layer, SiO_2 was reduced and Ti_3Si_5 was formed. The residual O was solved in the Ti–Al layer on top of the Ti–Si and locally led to the formation of Al_2O_3. EDX measurements at individual positions showed that a N peak was still found at the regions of the former barrier layers.

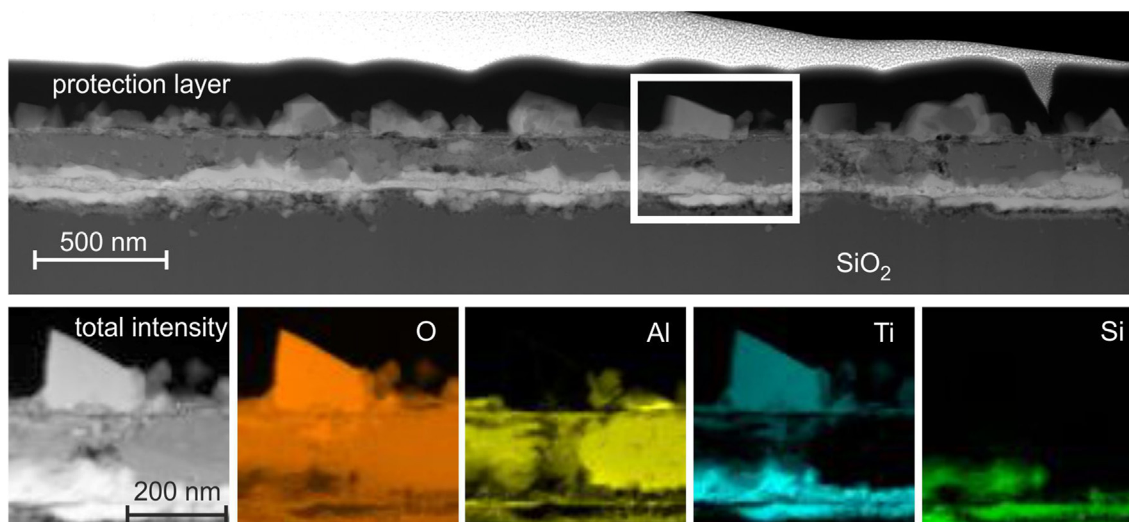

Fig. 9 – Overview STEM image (predominant elemental contrast) and EDX intensity mapping of an evaporated Ti/Al ML with 10 nm individual layer thickness on SiO_2/Si with an AlNO barrier and cover layer after annealing at 800 °C in HV.

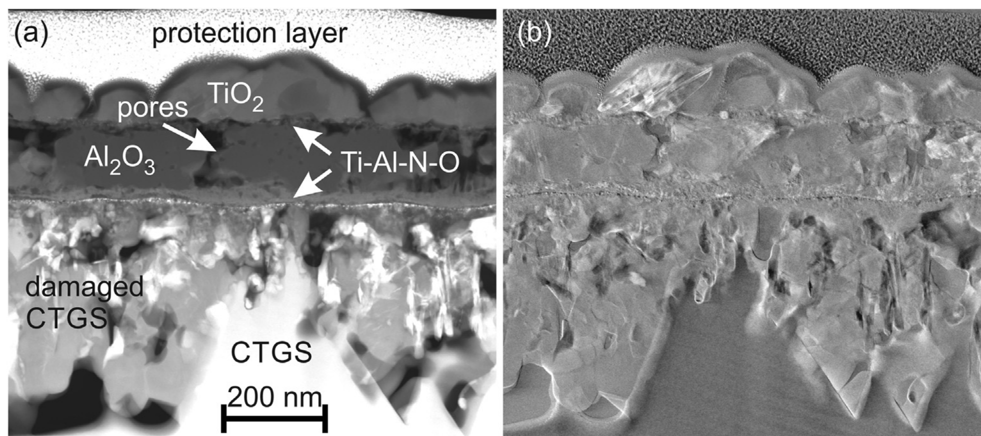

Fig. 10 – STEM images with (a) predominant elemental and (b) predominant orientation contrast of an evaporated Ti/Al ML sample on CTGS with 10 nm individual layer thickness after annealing at 800 °C in HV.

In Fig. 10 STEM images of an evaporated sample with 10 nm individual layer thickness on CTGS after annealing at 800 °C in HV are shown. As for the film on SiO_2/Si, TiO_2 grains were present at the film surface, while in the region of the former Ti–Al layer Al_2O_3 and pores were found. Locally, the TiO_2 grains on top of the surface include some Al_2O_3. On top of the substrate, a layer consisting of Ti, Al, O, and N was detected. At the interface, between the former Ti–Al and the AlNO cover layer, small grains with this composition are found as well. This means, that the N remained at its initial position also for these samples. The Ti signal in these layers was again explained by the above mentioned reaction between AlNO and Ti, which led to the formation of Ti–N.

The CTGS was degraded up to a depth of about 1 μm. The composition varied strongly and pores were present as well. EDX additionally revealed that Ti diffused about 50–100 nm into the substrate.

4. Discussion

The results presented above reveal a different high-temperature behavior of the sputtered as compared to the evaporated Ti/Al films.

The sputtered films showed a strong formation of the γ-TiAl phase in case of the SiO_2/Si substrates and at least a weak one on CTGS. They remained stable even after annealing at 800 °C in HV – on SiO_2/Si without, on CTGS with a weak oxidation.

In contrast to this, the phase formation of the evaporated films was less pronounced. Independent on the substrate, the films were completely oxidized after annealing at 800 °C in HV. Experiments with co-sputtered and co-evaporated Ti–Al films without a cover layer deposited on CTGS with a W adhesion layer already showed that after annealing at 600 °C in HV the co-sputtered films were only slightly oxidized at the sample surface. In contrast to this, the co-evaporated samples were already oxidized to a large extend (Fig. 11).

The main difference in film preparation by sputtering and e-beam evaporation is the energy of the impinging particles. This energy is in the range of a few eV in case of sputtering. The high energy results in a high mobility of the arriving atoms on the surface of the growing film, which leads to two effects. On the one hand, there is a high density of the grown film. On the other hand, the high atom mobility facilitates or even is a prerequisite to realize a crystallographic ordering of the atoms.

In the case of the evaporation methods, the energy of the particles is in the order of only 0.1 eV. This low energy hardly allows any mobility of the particles on the surface of the

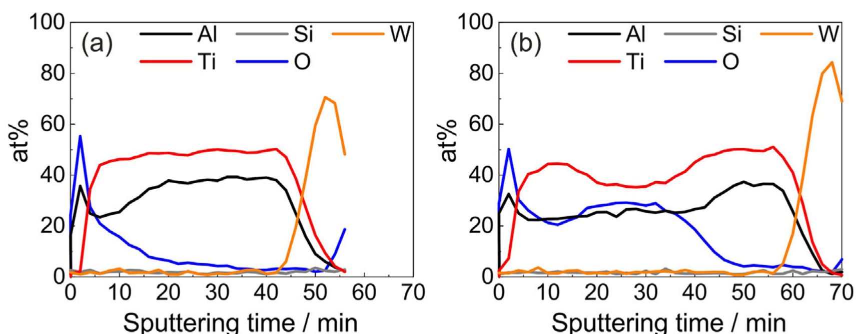

Fig. 11 – Results of the AES measurements of (a) a co-sputtered and (b) a co-evaporated Ti–Al film on CTGS covered with a W adhesion layer after annealing at 600 °C in HV.

growing film in case of a non-heated substrate during deposition. The films have a lower density and more defects. The crystallographic ordering is reduced.

The annealed evaporated films investigated in the present work contained pores (see SEM images in Fig. 8), which were absent in the sputtered samples (see SEM images in Fig. 2). This finding is explained by the higher density of vacancies generally present within the evaporated films, which coalesce during the heat treatment.

The influence of the deposition technique on the sample properties was investigated by several authors. Alvarez et al. [28] and Arshi et al. [29] analyzed the growth of Ti nanorods and extended films, respectively, prepared by the two techniques. Alvarez et al. [28] distinguished between three different growth regimes in dependence on the growth energy, where sputtered samples achieved a much higher density than the samples prepared with the low-energy deposition technique. Arshi et al. [29] found a different texture and crystal structure of the samples prepared by evaporation and sputtering. However, both films in their experiments had different thicknesses, which also might have been the reason for the different observed behavior.

Garbacz et al. [30] analyzed Al coatings with a thickness of several μm prepared either by vacuum evaporation or magnetron sputtering on Ti–6Al–4V alloy substrates. They observed that the films prepared by sputtering had a stronger texture and were more homogeneous. The evaporated films contained pores and were less homogeneous. The authors came to the conclusion that sputtered films are more suited for the preparation of diffusive Ti–Al intermetallic coatings.

The oxidation processes of Ti–Al samples were investigated by several authors. Taniguchi et al. [31] described the formation of a TiO_2 scale on the surface of the sample, below which Al_2O_3 and TiO_2 grains are present. Kekare and Aswath [32] stated that depending on the conditions and composition of the Ti–Al alloy, either Al or Ti oxidize preferentially. There is a faster diffusion of Ti than of O in rutile, whereas Al diffuses slowly in alumina [32]. Therefore, TiO_2 growths outwards, and the growth of Al_2O_3 is directed inside the sample. Rahmel and Spencer [33] also summarized conditions for the higher stability of Al_2O_3 or TiO_2.

In our former work on Ti–Al thin films we found that in the first step Al was oxidized [17]. After annealing at 800 °C in HV, in the thin Ti–Al films with SiO_2 cover layer all Al reacted to Al_2O_3, while Ti was still present as a Ti silicide and was not oxidized. This was different for the Ti–Al samples with AlNO cover and barrier layer investigated in the present work after annealing at 800 °C in HV. Here, we found TiO_2 grains at the surface of the sample and Al_2O_3 in the region of the former Ti–Al film (see Fig. 9), which was in agreement with the findings described by Taniguchi et al. [31] as well as Kekare and Aswath [32].

Zhang et al. [34] analyzed the oxidation behavior of evaporated and sputtered Ti films with a thickness of 150 and 100 nm. They found that the crystal structure of the TiO_2 formed by thermal oxidation depended on the deposition method. The rutile TiO_2 was formed at lower temperatures in the evaporated films as compared to the sputtered ones. They ascribed this behavior to the different microstructures of the as-deposited samples, for which they also found a different preferred texture.

The differences in the behavior of the sputtered and evaporated Ti/Al ML samples observed in the present work are in agreement with the findings reported in literature.

The AlNO barrier layers, which contain less O (8 at%), obviously are not suited as an oxidation protection since the evaporated Ti–Al samples were already partly oxidized after annealing at 600 °C in air and were completely destroyed after annealing at 800 °C in HV.

5. Summary and conclusions

This paper reports on the high-temperature stability of 200 nm thin Ti–Al films deposited on the high-temperature stable piezoelectric $Ca_3TaGa_3Si_2O_{14}$ (CTGS) substrates, which are investigated to determine their suitability for application as electrodes in surface acoustic wave (SAW) devices operating at high temperatures. The films were prepared as Ti/Al multilayer samples by two different deposition techniques, which were carried out at room temperature: sputtering and e-beam evaporation. As protection and barrier layers, sputtered AlNO thin films (20 nm) were used. The results revealed that the γ-TiAl phase formation was stronger in the sputtered films as compared to the evaporated ones. A comparison with Ti–Al films deposited on thermally oxidized Si substrates with SiO_2 cover layer, which were analyzed in former work, showed that the AlNO cover layer is much more suited as an oxidation protection. There was no degradation of the sputtered Ti–Al films with AlNO barriers even during annealing at 800 °C in HV, which was not realized with the SiO_2 cover. A slight oxidation of the sputtered Ti–Al films with AlNO barrier took place on the CTGS substrates. The evaporated Ti–Al films completely degraded after annealing at 800 °C in HV. On the one hand, this might be due to the reduced phase formation in these films and with this a potentially stronger affinity of Ti and Al to oxygen as compared to the elements bound in the γ-TiAl phase. On the other hand, the less protective AlNO cover layer with the reduced O content might be the reason.

In summary, sputtered Ti/Al multilayers have the potential to be applicable as a metallization for electrodes in SAW devices operating at elevated temperatures due to the better phase formation and HT stability. However, if the lift-off technique has to be applied for structuring, the evaporated samples can be used. They promise an application temperature of up to 600 °C. As a conclusion, TiAl is suggested as an alternative metallization system to Pt with the benefits of strongly reduced costs and a much lower density allowing different device designs.

Data availability

The raw/processed data required to reproduce these findings can be shared upon reasonable request.

Declaration of Competing Interest

The authors declare that they have no known competing financial interests or personal relationships that could have appeared to influence the work reported in this paper.

Acknowledgements

The work was supported by Germany BMBF under grant InnoProfile-Transfer 03IPT610Y and BMWI under grant 03ET1589 A. The authors gratefully acknowledge Erik Brachmann for the support of the sample preparation, Thomas Wiek as well as Dina Bieberstein for FIB cuts and TEM lamella preparation and Steffi Kaschube for AES and XPS measurements. Dina Bieberstein is also acknowledged for the support of the texture measurements.

REFERENCES

[1] Bewlay BP, Nag S, Suzuki A, Weimer MJ. TiAl alloys in commercial aircraft engines. Mater A T High Temp 2016;33(4–5):549–59.

[2] Rugg D, Dixon M, Burrows J. High-temperature application of titanium alloys in gas turbines. Material life cycle opportunities and threats – an industrial perspective. Mater A T High Temp 2016;33(4–5):536–41.

[3] Hornsteiner J, Born E, Riha E. Langasite for high temperature surface acoustic wave applications. Phys Status Solidi 1997;163(1):R3–4.

[4] Thiele JA, da Cunha MP. Platinum and palladium high-temperature transducers on langasite. IEEE Trans Ultrason Ferroelectrics Freq Contr 2005;52(4):545–9.

[5] da Cunha MP, Lad R, Moonlight T, Bernhardt G, Frankel D. High temperature stability of langasite surface acoustic wave devices. Ultrason Symp 2008:205–8.

[6] Aubert T, Elmazria O, Assouar B, Bouvot L, Hehn M, Weber S, et al. Behavior of platinum/tantalum as interdigital transducers for SAW devices in high-temperature environments. IEEE Trans Ultrason Ferroelectrics Freq Contr 2011;58(3):603–10.

[7] Richter D, Sakharov S, Forsén E, Mayer E, Reindl L, Fritze H. Thin film electrodes for high temperature surface acoustic wave devices. Procedia Engineering 2011;25:168–71.

[8] Moulzolf SC, Frankel DJ, da Cunha MP, Lad RJ. High temperature stability of electrically conductive Pt–Rh/ZrO_2 and Pt–Rh/HfO_2 nanocomposite thin film electrodes. Microsyst Technol 2014;20(4–5):523–31.

[9] Liu X, Peng B, Zhang W, Zhu J, Liu X, Wei M. Novel AlN/Pt/ZnO electrode for high temperature SAW sensors. Materials 2017;10(1):69.

[10] Weng H, Duan FL, Xie Z, Liu S, Ji Z, Zhang Y. $LiNbO_3$-Based SAW sensors capable to measure up to 1100 °C high temperature. IEEE Sensor J 2020;20(21):12679–83.

[11] Taguett A, Aubert T, Elmazria O, Bartoli F, Lomello M, Hehn M, et al. Comparison between Ir, $Ir_{0.85}Rh_{0.15}$ and $Ir_{0.7}Rh_{0.3}$ thin films as electrodes for surface acoustic waves applications above 800 °C in air atmosphere. Sensor Actuator Phys 2017;266:211–8.

[12] Menzel SB, Seifert M, Priyadarshi A, Rane GK, Park E, Oswald S, et al. Mo-La_2O_3 multilayer metallization systems for high-temperature surface acoustic wave sensor devices. Materials 2019;12(17):2651.

[13] Rane G, Seifert M, Menzel S, Gemming T, Eckert J. Tungsten as a chemically-stable electrode material on Ga-containing piezoelectric substrates langasite and catangasite for high-temperature SAW devices. Materials 2016;9(2):101.

[14] Seifert M, Rane GK, Menzel SB, Gemming T. The influence of barrier layers (SiO_2, Al_2O_3,W) on the phase formation and stability of RuAl thin films on LGS and CTGS substrates for surface acoustic wave technology. J Alloys Compd 2016;688:228–40. Part A.

[15] Seifert M, Rane GK, Menzel SB, Oswald S, Gemming T. Improving the oxidation resistance of RuAl thin films with Al_2O_3 or SiO_2 cover layers. J Alloys Compd 2019;776:819–25.

[16] Seifert M. High temperature behavior of RuAl thin films on piezoelectric CTGS and LGS substrates. Materials 2020;13(7):1605.

[17] Seifert M, Lattner E, Menzel SB, Oswald S, Gemming T. phase formation and high-temperature stability of very thin Co-sputtered Ti-Al and multilayered Ti/Al films on thermally oxidized Si substrates. Materials 2020;13(9):2039.

[18] Streque J, Camus J, Laroche T, Hage-Ali S, M'Jahed H, Rammal M, et al. Design and characterization of high-Q SAW resonators based on the AlN/sapphire structure intended for high-temperature wireless sensor applications. IEEE Sensor J 2020;20(13):6985–91.

[19] Yu F, Zhang S, Zhao X, Yuan D, Qin L, Wang Q-m, et al. Investigation of $Ca_3TaGa_3Si_2O_{14}$ piezoelectric crystals for high-temperature sensors. J Appl Phys 2011;109(11):114103.

[20] Seifert M, Menzel SB, Rane GK, Hoffmann M, Gemming T. RuAl thin films on high–temperature piezoelectric substrates. Mater Res Express 2015;2(8):085001.

[21] MultiPak, software package, V. 9.5, ULVAC-PHI, 1994–2014.

[22] Oswald S, Lattner E, Seifert M, Menzel S. AES and XPS depth-profiling of annealed AlN/Ti-Al/AlN films for high-temperature applications in SAW metallization. Surf Interface Anal 2018:1–5 (0).

[23] Brien V, Pigeat P. Correlation between the oxygen content and the morphology of AlN films grown by r.f. magnetron sputtering. J Cryst Growth 2008;310(16):3890–5.

[24] Pinkas M, Frage N, Froumin N, Pelleg J, Dariel MP. Early stages of interface reactions between AlN and Ti thin films. J Vac Sci Technol, A 2002;20(3):887–96.

[25] He X, Yang S-Z, Tao K, Fan Y. Investigation of the interface reactions of Ti thin films with AlN substrate. J Mater Res 1997;12(3):846–51.

[26] Lazar P, Redinger J, Strobl J, Podloucky R, Rashkova B, Dehm G, et al. N-K electron energy-loss near-edge structures for TiN/VN layers: an ab initio and experimental study. Anal Bioanal Chem 2008;390(6):1447–53.

[27] Pankov VV, P RH, Coullard M, Botton GA. Transmission electron microscopy of AlN/TiN superlattice coatings fabricated by pulsed laser deposition. Inst Phys Conf 2003;180.

[28] Alvarez R, Garcia-Valenzuela A, Rico V, Garcia-Martin JM, Cotrino J, Gonzalez-Elipe AR, et al. Kinetic energy-induced growth regimes of nanocolumnar Ti thin films deposited by evaporation and magnetron sputtering. Nanotechnology 2019;30(47):8.

[29] Arshi N, Lu J, Lee CG, Yoon JH, Koo BH, Ahmed F. Thickness effect on properties of titanium film deposited by d.c. magnetron sputtering and electron beam evaporation techniques. Bull Mater Sci 2013;36(5):807–12.

[30] Garbacz H, Wiecinsky P, Adamczyk-CieslakB, Mizera J, Kurzydlowsk KJ. Studies of aluminium coatings deposited by vacuum evaporation and magnetron sputtering. J Microsc 2010;237(3):475–80.

[31] Taniguchi S, Shibata T, Itoh S. Oxidation behavior of TiAl at high temperatures in purified oxygen. Mater Trans, JIM 1991;32(2):151–6.
[32] Kekare SA, Aswath PB. Oxidation of TiAl based intermetallics. J Mater Sci 1997;32(9):2485–99.
[33] Rahmel A, Spencer PJ. Thermodynamic aspects of TiAl and TiSi2 oxidation: the Al-Ti-O and Si-Ti-O Phase diagrams. Oxid Metals 1991;35(1):53–68.
[34] Zhang Y, Ma X, Chen P, Yang D. Crystallization behaviors of TiO_2 films derived from thermal oxidation of evaporated and sputtered titanium films. J Alloys Compd 2009;480(2):938–41.